COMMUNICATIONS PHYSICS

ARTICLE

https://doi.org/10.1038/s42005-019-0129-5 OPEN

Correlating anisotropic mobility and intermolecular phonons in organic semiconductors to investigate transient localization

Emily G. Bittle[1], Adam J. Biacchi[1], Lisa A. Fredin[2,4], Andrew A. Herzing[3], Thomas C. Allison[2], Angela R. Hight Walker[1] & David J. Gundlach[1]

Developing a fundamental understanding of charge transport in organic semiconductors has been a decades-long challenge that hinders performance improvement. In particular, recent work suggests that organic semiconductors have unique charge–phonon interactions where phonons temporarily interrupt the band structure causing a transient localization of charge carriers. Despite growing evidence to support this mechanism, further understanding and control will depend on pinpointing the molecular motions that cause substantial change to the band structure. Here we combine experimental and theoretical techniques to demonstrate the phonon energies and associated molecular motions governing the charge–phonon interaction in single crystal tetracene. We investigate phonon properties using polarized Raman spectroscopy, transmission electron microscopy, and density functional theory, and correlate this with the anisotropic mobility. We find that specific phonons disrupt the band orbital in the high-mobility direction, evident in the discrepancy between measured and static calculations of the mobility anisotropy ratio in tetracene.

[1] National Institute of Standards and Technology, Nanoscale Device Characterization Division, 100 Bureau Drive, Gaithersburg, MD 20899, USA. [2] National Institute of Standards and Technology, Chemical Sciences Division, 100 Bureau Drive, Gaithersburg, MD 20899, USA. [3] National Institute of Standards and Technology, Materials Measurement Science Division, 100 Bureau Drive, Gaithersburg, MD 20899, USA. [4] Present address: Department of Chemistry, Lehigh University, 6 E. Packer Ave., Seeley G. Mudd, Bethlehem, PA 18015, USA. Correspondence and requests for materials should be addressed to E.G.B. (email: Emily.Bittle@nist.gov)

Competing energetic pathways for charge conduction in organic semiconductors result in a range of behavior from hopping to band-like depending on molecular energetics and packing. Traditional semiconductor physics models often fail to predict organic semiconductor device behavior because usual simplifications that consider hopping and band transport mechanisms separately are not applicable. In addition, many extrinsic factors influence the measured transport in a device, such as interface traps[1] and contact resistance[2,3], resulting in ambiguous and sometimes conflicting results. For example, temperature-dependent transistor mobility, μ_{FET}, commonly used to determine the transport physics, is highly influenced by device structure[4,5] leading to inconsistent results for the same crystalline organic semiconductor[6,7]. Some advanced electrical studies on small-molecule, single crystals and high-performing polymers (transistor mobility $\mu_{FET} \approx 10\ cm^2/Vs$) show signatures of band-like behavior suggesting that extended state conduction may exist. However, measurements of Hall mobility, in which the signal arises from charge momentum and therefore is indicative of band structure, are notoriously weak in organic semiconductors[8,9] as band conduction does not appear to be the only, or dominant, transport mechanism even in high-performing materials. All of this has prevented a clear understanding of charge conduction in organic materials.

In addition to the convolution of band and hopping mechanisms, intermolecular motions within the crystal lattice, i.e., phonons, can be disruptive to transport. Due to the weak bonding between molecules in organic semiconductors, phonons can change the coupling between neighboring molecular orbitals. This "dynamic disorder" is theorized to cause a significant change to the local environment of charge carriers at energies close to those important to electrical transport, such as the intermolecular transfer integral (J) and the polaron energy (E_p), in an effect known as transient localization[10–12]. Several studies have correlated increased amplitude of intermolecular motions with decreased electrical performance using either direct measurement of molecular motion or by suppressing motion using strain or decreased temperature during electrical measurement[13–18]. The reported results suggest that transient localization due to phonons is influential on device performance and may explain the lack of clearly defined band-like conduction in highly ordered, close-packed organic semiconductors.

In the transient localization framework, phonons can be more or less influential on transport depending on the direction and magnitude of the molecular motion in relation to the orientation of the neighboring orbitals[12,19]. Both phonons and charge transport in single crystals have distinct directionality such that the impact of specific phonons on charge transport is accessible to both experimental and theoretical studies. As a step toward crafting a fundamental charge conduction model for organic semiconductors, we establish connections between specific phonons and charge transport in one material. To probe this relationship, we correlate anisotropic field-effect mobility with measures of phonons using polarized Raman spectroscopy and transmission electron microscopy (TEM). The single crystal is modeled using periodic boundary condition density functional theory (DFT). The calculations are used to identify measured phonons, establish the directionality of the associated molecular and lattice motions, and predict the changes to electrical interactions for the observed phonons. We correlate the directionality of the associated molecular motion with the high- and low-mobility axes measured in-plane. By doing so, we provide a clear connection between intermolecular motions and charge transport.

Results

Single crystal tetracene as a test case. Single-crystal measurements have long been the foundation of fundamental organic semiconductor transport studies[20]. The high degree of order provides a uniform, predictable energetic landscape, and the results can be extended to understand transport within grains of polycrystalline samples and the impact of packing structures. Previous experimental characterization of a single crystal tetracene shows evidence of charge carrier mechanisms associated with both hopping and band-like mobility. Temperature dependence of μ_{FET} using a single crystal over an air-gap dielectric shows an activated dependence, characteristic of hopping[7], while an earlier study on the SiO_2 dielectric shows that μ_{FET} decreases with temperature, characteristic of band conduction[6]. Tetracene has a Hall signal[8] which is only possible for charge delocalized in a band, and $\mu_{FET} > 1\ cm^2/Vs$[21,22]. Tetracene, therefore, is a good test case to elucidate how high- and low-performance mechanisms combine in ordered, small-molecule organic semiconductors and how this is affected by phonons. An additional benefit of our study is that we have made complimentary measurements on the same crystal of tetracene, or in the case of TEM, on crystals from the same growth batch.

We grow tetracene single crystals using the physical vapor technique common in single-crystal small-molecule organic semiconductor studies[23,24] producing crystals that are on the order of 0.5 mm in the facile charge transport *ab*-plane and 0.3 −1.5 μm perpendicular to this. Tetracene crystals preferentially form a triclinic crystal with P-1 symmetry with two molecules per unit cell and arrange in a herringbone structure in the *ab*-plane, Fig. 1a. The *ab*-plane growth edges do not consistently orient with respect to the principal axes. Due to this, determining the orientation within this plane in tetracene single crystals requires careful measurement and cannot be done by aligning the long and short growth edges, as is done with rubrene[25]. To determine the crystal orientation, we matched the polarized photoluminescence (PL) and polarized Raman measurements on the transistor single crystal with that of a crystal where the orientation was known from TEM-selected area diffraction measurement, Fig. 1b and c. The polarized PL signal measured at 531 nm is correlated with the short axes of the tetracene molecule, and thereby aligns ~9° from the [010][26]. For propagation through thicker crystals, this signal has been shown to have a small component in the [100] direction that is consistent with our results for the transistor sample[26].

Anisotropic mobility in tetracene. Figure 2a shows the mobility anisotropy of a single crystal tetracene transistor measured at room temperature using a circular pattern of contacts shown in Fig. 2b. The highest mobility measured aligns most closely with the [−110]/[1−10] direction, and the lowest mobility is approximately perpendicular to this. The anisotropy ratio between the highest and lowest measured mobility is approximately $\mu_H/\mu_L \approx 1.5$ to 2, similar to the results found by Xia et al.[7]. Details of the mobility extraction are included in Supplementary Note 1 and Supplementary Figs. 2–5.

Mobility anisotropy in organic semiconductors is tied to their crystal structure[27–29]. Tetracene shows mobility anisotropy typical of other herringbone-layered organic semiconductors such as pentacene[30] and rubrene[31,32]. P-type mobility depends on the highest-occupied molecular orbital (HOMO) overlap that is dependent on close, face-to-face orientation of the aromatic rings. The *c*-axis mobility is lower than the *ab*-plane mobility due to the layered structure, Supplementary Fig. 1(a). Within the *ab*-plane, we calculate the HOMO for a cluster of seven molecules out of the optimized periodic crystal *ab*-plane, Fig. 2c. The calculation demonstrates the electrical interactions between molecules, which results in the sharing of charge carriers. Calculation for the optimized crystal shows that the cluster HOMO forms a band

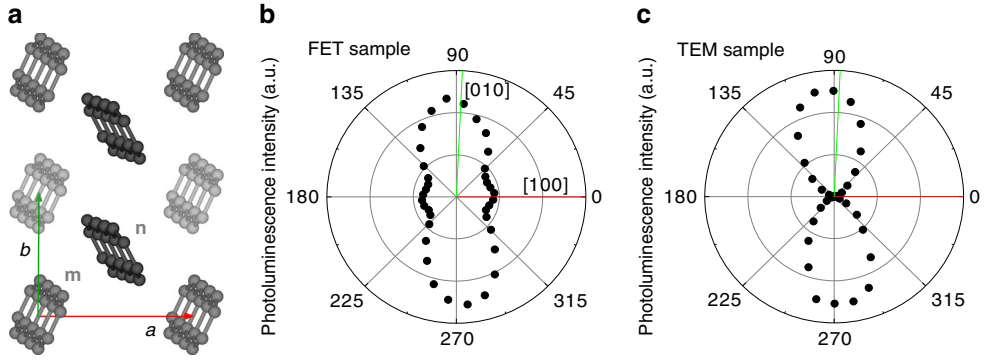

Fig. 1 Crystal structure and orientation in the *ab*-plane of tetracene. **a** Crystal structure, hydrogen atoms not shown. Red (horizontal) axis is *a*, green axis is *b*. Two molecules, **m** and **n**, make up the unit cell. **b** Polarized photoluminescence measured at 531 nm using 514-nm excitation of the sample used for transistor (**b**) and transmission electron microscopy (**c**) measurements. Data are rotated so that the *a* axis/[100] direction aligns with 0°

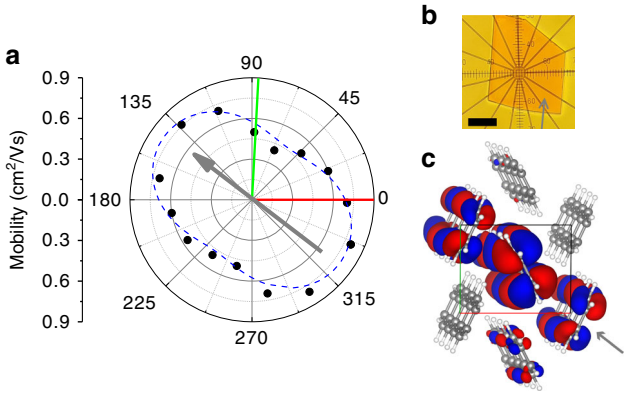

Fig. 2 Anisotropic mobility in tetracene. **a** Saturation transistor mobility anisotropy measured in a single crystal field-effect transistor, the dashed line is an empirical fit. Data are aligned such that the crystalline [100] direction is at 0° (red line) and the [010] direction is at ~87° (green line). Data are typical in magnitude of mobility and shape measured over nine samples of lengths $L = 5$, 10, 20, and 40 μm. **b** Micrograph of a transistor measured for mobility in plot (**a**) and polarized Raman; channel length $L =$ 5 μm. Scale bar shows 100 μm. **c** Highest-occupied molecular orbital (HOMO) calculated for a seven-molecule cluster in the neutral crystal structure. The [−110] direction indicated by a gray arrow in all parts of the figure

which lies along the [−110] direction, matching the high-mobility direction from experiments. Optimized lattice parameters used for the calculation are given in Supplementary Table 1. Previous calculations of mobility anisotropy in tetracene predict $\mu_H/\mu_L > 10$ in the *ab*-plane[33,34], much higher than our measured values and those reported by Xia et al.[7]. This discrepancy may be explained by anisotropic charge–phonon interactions, as suggested by a study of rigid molecule motions in pentacene and rubrene by Isii et al.[35]. We therefore investigate this in the context of directionally oriented charge–phonon interactions in tetracene.

Impact of molecular motion on charge transport. To determine the influence of molecular motions on transport in the *ab*-plane, we measure the intermolecular phonons using polarized Raman and TEM and identify them using calculations. The selection rules for each measurement are different, resulting in complementary datasets. Raman signal requires a change in polarizability and TEM requires correlated molecular displacements from the static lattice. We find that the tetracene Raman modes identified in this study are associated with rocking motion, and TEM streaking likely arises from a bending motion. Below, we discuss the details of the motion and impact on charge transport.

Raman-active phonons. At low frequencies (< 200 cm^{-1}), organic crystals have Raman-active modes associated with intermolecular phonons that are occupied at ambient conditions (≈25 meV). We investigate Raman-active phonons shown in Fig. 3a along with the calculated Raman-active transitions for the single molecule and for the crystal in the low- and mid-frequency region. Details of the Raman experimental parameters are in the Methods section. To identify the phonons contributing to the low-frequency Raman shifts, we need to model both the periodic structure and the weak intermolecular interactions. Thus, we use DFT in an atom-centered basis set and periodic boundary conditions to calculate the optimized lattice parameters and normal mode phonons. Raman-active modes in the mid-frequency (fingerprint) region appear in both single-molecule and crystal calculations, demonstrating that these are primarily due to intramolecular motions. Two low-frequency modes at 118.4 cm^{-1} and 130.7 cm^{-1} (14.7 meV and 16.2 meV) appear only in the crystal calculation, indicating that these are intermolecular phonons. Vector diagrams showing the molecule motions associated with the calculated low-frequency Raman-active phonons are shown in Fig. 3b and Supplementary Movies 1 and 2. The primary motion associated with mode I at 118.4 cm^{-1} aligns most strongly with the [100] and [010] directions. The oscillation does not show large shifts in the neighboring molecular distances in the high- or low-mobility directions.

The motion associated with mode II at 130.7 cm^{-1} is most intense in the [−110] and [110] directions, which align with the high- and low-mobility directions, respectively. We measure the parallel polarized signal for mode II to gain insight into the orientation of the polarizability, Fig. 3c. All Raman-active modes for a P-1 crystal have A_g symmetry, such that each mode has a primary axis and will show symmetric lobes in parallel polarized Raman collection. Because of the crystal growth habit, the incident light is canted with respect to the *c*-axis, as shown in Supplementary Fig. 1 and discussed in the Methods section, such that additional lobes are apparent. The calculated Raman parallel-polarization intensity (shown in blue) has primary lobes in the [−110] and [110] directions; the much smaller intensity of the [110] lobes is underestimated with respect to experiments in the perfect crystal calculations. The high intensity of the side lobes in an experiment may originate from crystal tilt with respect to the light path, the increased pathlength of the light through the crystal thickness (calculations are performed for one molecular

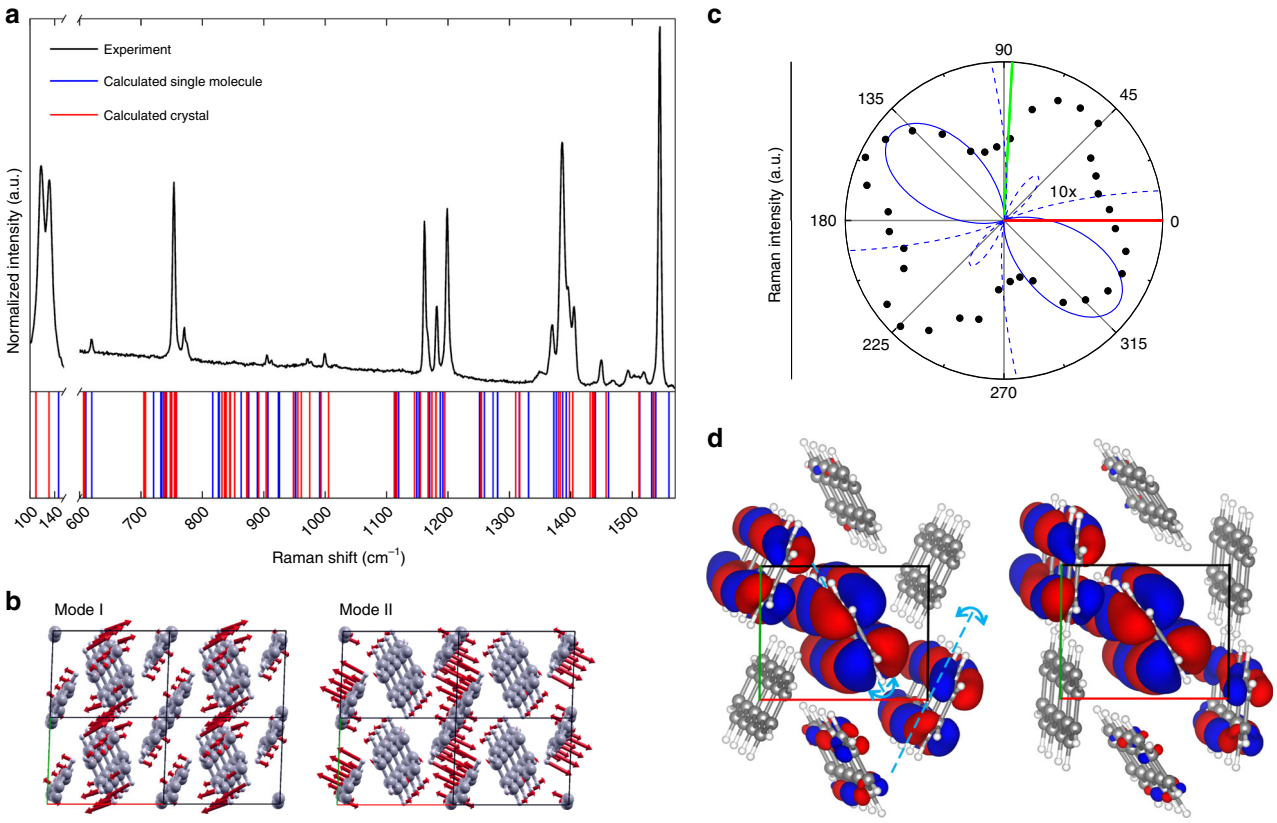

Fig. 3 Phonons identified by Raman spectroscopy of tetracene. **a** Raman spectrum of a single crystal tetracene. **b** Diagrams illustrate the motion vectors of the atoms for mode I (118.4 cm^{-1}) and II (130.7 cm^{-1}). **c** Parallel polarized Raman intensity for mode II, wavenumber $\nu = 130.7\ cm^{-1}$, of a single crystal tetracene (solid dots) measured with 785-nm excitation on the crystal used for transistor measurements. Normalized calculated polarization intensity is shown in blue, solid lines scaled to data and dotted are 10× larger. **d** Highest-occupied molecular orbital for the seven-molecule cluster at minimum (left) and maximum (right) of the displacement of mode II at 300 K. Cyan arrows indicate the rocking motion of the molecules. The red axis (horizontal) is the [100] and the green axis is the [010] direction in (**c**) and (**d**)

layer), or ambiguity in defining the intensity in calculations. For comparison, the same crystal measured on a single-grating spectrometer and on the crystal used for TEM measurement is shown in Supplementary Fig. 6 and shows diminished side lobes as compared to Fig. 3c.

We calculate the HOMO for a cluster of seven molecules in the *ab*-plane at several positions between the maximum and minimum of the mode II motion predicted near room temperature (300 K) to probe the effect on charge transport. As seen in Fig. 3d, Supplementary Fig. 7, and Supplementary Movie 3, the rocking motion associated with Raman mode II results in subtle changes to the cluster HOMO. In the [110] (low-mobility) direction, the nearest neighbors move to a more face–face orientation that is expected to lead to higher mobility as the transport essential pi-orbitals extend from the face of the molecule, but this motion also moves the orbitals on neighboring molecules further away from each other, resulting in lower interaction along this direction. In the [−110] (high-mobility) direction, the rocking leads to a closer configuration between the edges of the two molecules of the unit cell. At maximum displacement, this results in slight localization of the HOMO in the [−110] direction indicating weakening of the band orbital and a transient transition to hopping transport in the high-mobility direction.

TEM phonon. As shown previously[13,14], TEM can be used to detect large-amplitude vibrational motions in organic crystals by the presence of diffuse, directional streaks in the diffraction pattern. Illig et al.[13] showed that the relative amount of streaking, as a proxy for molecular motion, is correlated with the device mobility in several different small-molecule organic semiconductors[14]. In Fig. 4a, we see a similar faint streaking in the [110] direction, close to the low-mobility direction of a tetracene single crystal at room temperature. Similar to the results for dinaphtho[2,3-b:2′,3′-f]thieno[3,2-b]thiophene (DNTT)[13], tetracene is expected to have a very low amount of TEM streaking due to its rigid packing structure. From our phonon calculations, we considered molecular displacement calculated from the force vectors (eigenvectors) associated with each calculated normal mode near room temperature (300 K) to assign a phonon mode to the streaking. The motions that can produce this TEM streaking must have a relatively large molecular displacement along the [110] direction due to the molecular orientation with respect to the streak pattern[14] and relatively little change in other directions. The calculated force vectors for each mode provide a relative measure of how each atom in the system is oscillating, and thus the change in lattice plane spacing can be estimated as the change in the centers of mass of the two molecules in the unit cell, labeled **m** and **n** in Fig. 1a. The magnitude of the variations of the centers of mass projected along the [110] direction was quantified for all the normal modes. An IR-active mode at 100.53 cm^{-1}, mode III, results in a molecular center of mass displacement of 0.16 Å along the [110] direction at room temperature, which is ≈43% more than any other mode. We therefore assign this phonon to the TEM streaking. The displacement vectors for mode III are shown in Fig. 4b, Supplementary Movie 4, and the center of mass displacement is shown in Supplementary Fig. 8.

Figure 4c, Supplementary Fig. 9, and Supplementary Movie 5 show that the predicted TEM mode III causes a disruption of the cluster HOMO along the high-mobility direction. In the frame of

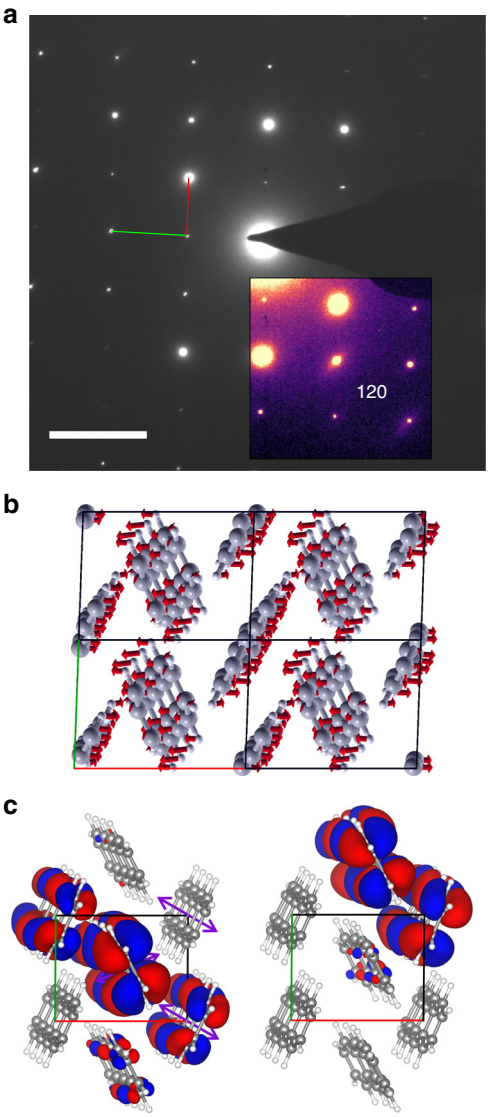

Fig. 4 Phonon identified in transmission electon microscopy (TEM) of tetracene. **a** TEM diffraction pattern of a single crystal tetracene at room temperature. False color image enhances the streaking pattern seen at 120. Scale bar shows 2 nm^{-1}. **b** Motion vectors of the atoms for mode III. **c** Highest-occupied molecular orbital (HOMO) for the seven-molecule cluster at minimum (left) and maximum (right) molecular displacement of mode III, correlated with streaking in TEM. The purple arrows show the direction of molecular bending, red and green lines indicated the *a* and *b* axes, respectively

the **n** molecules, the associated molecular bending motion results in an increased distance to the [−100] neighbor and a decreased distance to the [100] neighbor. Consequently, the HOMO shifts from delocalized sharing between the molecules along the [−110] direction in the neutral crystal to localization between m-n pairs of molecules at the maximum molecular displacement. This motion disrupts the band structure along the [−110] direction and we therefore identify that the mobility of tetracene is lowered due to transient localization in the high-mobility direction.

Discussion

The rocking and bending of molecules associated with phonons identified in tetracene along with the mobility directions are summarized in Fig. 5. In the static lattice, the HOMO for the cluster localizes along the [−110] direction and is redistributed

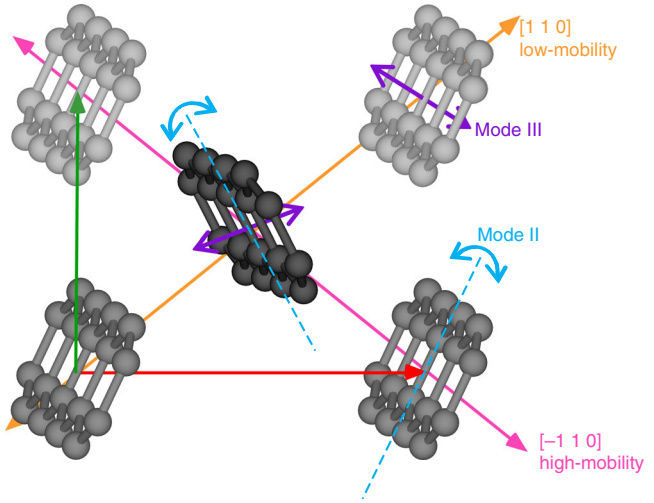

Fig. 5 Summary of results. Mobility and phonon directions in a single crystal tetracene

during motion, intermittently extending and contracting within the *ab*-plane. The two motions demonstrated here disrupt the orbital overlap in the high-mobility direction while also transiently changing the interaction in other directions. We show that mode II is a Raman-active phonon with molecular rocking motion that changes the shared crystal HOMO subtly, causing a localization along the high-mobility direction. Mode III observed using TEM has a molecular bending motion which changes the HOMO significantly and causes a breakdown of the band structure along the high-mobility direction. The redistribution of the HOMO band by the thermally occupied phonons is evident in the large discrepancy between the measured anisotropy ratio (≈2 ×) and calculations of this ratio from the static lattice (>10 ×).

In summary, we have correlated the anisotropic mobility in a single crystal tetracene with measured intermolecular phonons and HOMO cluster calculations to demonstrate how specific phonons impact charge transport. Our results highlight how charge transport can be directionally impacted by phonons in an organic molecular lattice. The molecular rocking motion (measured using Raman spectroscopy) causes slight localization of the intermolecular HOMO and large molecular bending (seen in TEM measurements) disrupts the HOMO band formed along the high-mobility direction. The lowered interaction between molecules (and therefore the lower charge transport) due to molecular motion along the high-mobility direction may cause the anisotropy ratio μ_H/μ_L to be lower than the value calculated for the static lattice, and this is observed in measured values. While the results here show a decrease in charge transport along the high-mobility direction, one can imagine a scenario in which phonons could result in increased intermolecular overlap, resulting in faster charge transport.

Furthermore, our results show that understanding the effects of transient localization benefits from experimental and theoretical investigation of charge transport and phonons along directions associated with larger relative changes to the electronic structure. The charge transport properties of organic semiconductors are known to be dependent on the packing structure, and the corresponding synthesis efforts have successfully produced materials which produce densely packed structures with high pi-orbital overlap. Future efforts to create organic semiconductors with high mobilities will benefit from a broader view, incorporating both the static molecular lattice and phonons. Understanding the transient localization capacity of different types of molecular motions will inform optimization of the dynamic lattice.

Methods

Tetracene single-crystal growth. Tetracene single crystals were grown by the physical vapor transport method[23,24]. The oven consists of quartz tubes wrapped with resistive wire to create a temperature gradient. Argon flow was set to 60 sccm, source temperature was ~245 °C, and temperature at the crystal growth site was ~200–220 °C. Crystals grown in a 45-min time frame were on the order of 50 μm to 1 mm on a side, and between 0.3- and 1.5-μm thick.

Tetracene field-effect mobility measurements. Field-effect transistor measurements were used to determine mobility along 15° increments within the *ab*-plane of a single crystal tetracene. Gate contact and dielectric were n-doped silicon covered by 50 nm of thermally oxidized silicon dioxide and a layer (≈ 70 nm) of fluoropolymer Cytop. Total capacitance of the composite dielectric was measured using an impedance meter and modeled as a parallel RC circuit to extract $C_{diel} = 1.88 \times 10^4$ F/m^2, as shown in Supplementary Fig. 4. Palladium contacts (30 nm) were then evaporated using photoresist masking; a 30-nm sacrificial aluminum layer was used to assist in the adhesion of the photoresist to the Cytop surface. The Al layer was removed from the contact area using a soak in a tetramethylammonium hydroxide-based photoresist developer. After Pd deposition, the remaining Al was removed using a 50 °C bath in a commercial aluminum remover. To decrease contact resistance between the tetracene and Pd, the substrate was soaked in a bath of pentafluorobenzenethiol in anhydrous ethanol for 2 h at 80 °C, and then rinsed with ethanol. After crystals were laminated, a thin coating of Cytop was used to encapsulate the device to reduce degradation.

Measurements of mobility were made using a commercial semiconductor parameter analyzer using adjacent contact pads as drain and source. The remaining contacts were allowed to float. Measurements were made in a nitrogen atmosphere in the dark. To remove artifacts arising from charging the neighboring drain–source pads, measurements were made at a slow rate of ~0.8 V/s. To remove biasing effects due to induced charge trapping in the neighboring channels, the gate was swept to a positive bias after each measurement. Contact resistance was estimated using the transfer length method and showed a slight gate voltage dependence, see Supplementary Fig. 3.

Density functional theory calculations. Full geometry optimization and vibrational spectra calculations of the tetracene single crystal were performed using the hybrid exchange-correlation functional, B3LYP, and a traditional double-zeta basis set, 6–31G(d,p), implemented for periodic boundary conditions (PBC) in CRYSTAL14[36]. In all calculations, a shrinking factor of 3 Hartrees and an energy convergence tolerance of 8 Hartrees were applied. Starting from the tetracene-labeled TETCEN[37] crystal structure, which was recorded at room temperature (RT) and is available from the Cambridge Structural Database (CSD)[38], led to a triclinic unit cell composed of two molecules with a P-1 space group with lattice parameters $a =$ 7.92 Å, $b = 5.96$ Å, and $c = 13.14$ Å, $\alpha = 98.79°$, $\beta = 108.25°$, and $\gamma = 87.33°$ (Supplementary Fig. 1). For comparison, the vibrational spectra of a single tetracene crystal were calculated using the same functional and basis set in vacuum using Gaussian09[39].

The Raman tensor elements were calculated using the Raman intensity option implemented in CRYSTAL14 based on the coupled perturbed Hartree–Fock/Kohn–Sham (CPHF/KS) method. Each Raman-active mode was visualized as the atomic displacement according to the movement for the individual phonon modes taken from the frequency calculation output. While comparing the experimental and DFT-computed Raman spectra, all computed frequencies and transitions have been scaled by the standard B3LYP/6–31G(d,p) scaling factor, 0.9613[40] (Fig. 3a).

The Raman intensity of a phonon mode can be written according to the classical Placzek approximation as[41]:

$$I \propto |\mathbf{e}_i \cdot \mathbf{R} \cdot \mathbf{e}_s|^2, \quad (1)$$

where $\mathbf{R}$ is the Raman tensor and $\mathbf{e}_i$ and $\mathbf{e}_s$ are the electric polarization unitary vectors of the incident and scattered light, respectively. Since all the Raman-active modes in a P-1 crystal have A_g symmetry, they all have Raman tensors of the form:

$$\mathbf{R} = \begin{pmatrix} a & d & e \\ d & b & f \\ e & f & c \end{pmatrix}. \quad (2)$$

Since the *ab*-plane of the crystal aligns with the largest flat edge on all crystals, the incident light is perpendicular to this plane. Aligning *a* with the *x*-axis, *b* is nearly aligned with the *y*-axis, and *c* is obtuse to the *ab*-plane, and the incident light is along the *z*-axis. Expanding the Raman modes in Cartesian coordinates, the [100] vector is aligned with the *x*-axis and by rotating the sample, an angle θ (counterclockwise rotation), such that the [010] vector is 270° with a fixed initial angle of θ_o of −15°, which yields $\mathbf{e}_i = \mathbf{e}_s = (\cos(\theta + \theta_o) \quad \sin(\theta + \theta_o) \quad 0)$ for the incident and scattered light in the parallel configuration.

This convention leads to the angular-dependent intensity expression for A_g modes:

$$I_{||} \propto \left|a + (b - a)\sin^2(\theta + \theta_o) + d\sin 2(\theta + \theta_o)\right|^2. \quad (3)$$

TEM measurements. Samples for TEM measurement were prepared by placing individual thin tetracene crystals (≈0.30 μm) onto an amorphous carbon on gold grid. Electron diffraction patterns were collected using an FEI Titan 80–300 transmission electron microscope using a beam energy of 300 keV. The patterns were collected using a multi-scan CCD detector (MSC KAF1000; Gatan, Inc.). In order to collect sufficient signal and prevent saturation of the CCD, 10 frames were summed using 0.1 s per frame exposure.

Raman and photoluminescence measurements. Raman spectra were collected at room temperature in the 180° backscattering configuration through a confocal microscope (×50 objective) coupled to a Horiba JY T64000 triple-grating Raman spectrometer (1800 lines/mm) equipped with a liquid nitrogen-cooled CCD detector. A 785-nm diode laser was employed for excitation and the power of the incident light was maintained at 5 mW. The laser was linearly polarized and the scattered light was collected through a polarizer set parallel to the incident polarization. The collection time was 300 s. PL spectra were obtained using a single-grating spectrometer (Renishaw inVia micro-Raman) using a ×50 objective and a 1200 lines/mm grating. The excitation source was a linearly polarized 514-nm Ar^+ laser (100 μW). Backscattered PL was collected through a polarizer set parallel to the incident polarization at a collection time of 1 s. For both Raman and PL analysis, the sample was rotated in increments of 10°.

Data availability

Data can be obtained by contacting the authors, or through the National Institute of Standards and Technology.

Received: 6 September 2018 Accepted: 5 February 2019
Published online: 19 March 2019

References

1. Un, H.-I. et al. Charge-trapping-induced non-ideal behaviors in organic field-effect transistors. *Adv. Mater.* **30**, 1800017 (2018).
2. Uemura, T. et al. On the extraction of charge carrier mobility in high-mobility organic transistors. *Adv. Mater.* **28**, 151–155 (2016).
3. Bittle, E. G., Basham, J. I., Jackson, T. N., Jurchescu, O. D. & Gundlach, D. J. Mobility overestimation due to gated contacts in organic field-effect transistors. *Nat. Commun.* **7**, 10908 (2016).
4. Mei, Y. et al. Crossover from band-like to thermally activated charge transport in organic transistors due to strain-induced traps. *Proc. Natl Acad. Sci. USA* **114**, E6739–E6748 (2017).
5. Nelson, S. F., Lin, Y. Y., Gundlach, D. J. & Jackson, T. N. Temperature-independent transport in high-mobility pentacene transistors. *Appl. Phys. Lett.* **72**, 1854–1856 (1998).
6. Boer, R. W. I., de, Klapwijk, T. M. & Morpurgo, A. F. Field-effect transistors on tetracene single crystals. *Appl. Phys. Lett.* **83**, 4345–4347 (2003).
7. Xia, Y., Kalihari, V., Frisbie, C. D., Oh, N. K. & Rogers, J. A. Tetracene air-gap single-crystal field-effect transistors. *Appl. Phys. Lett.* **90**, 174–176 (2007).
8. Chen, Y., Yi, H. T. & Podzorov, V. High-resolution ac measurements of the hall effect in organic field-effect transistors. *Phys. Rev. Appl.* **5**, 34008 (2016).
9. Yi, H. T., Gartstein, Y. N. & Podzorov, V. Charge carrier coherence and Hall effect in organic semiconductors. *Sci. Rep.* **6**, 23650 (2016).
10. Aragó, J. & Troisi, A. Regimes of exciton transport in molecular crystals in the presence of dynamic disorder. *Adv. Funct. Mater.* **26**, 2316–2325 (2016).
11. Fratini, S., Mayou, D. & Ciuchi, S. The transient localization scenario for charge transport in crystalline organic materials. *Adv. Funct. Mater.* **26**, 2292–2315 (2016).
12. Ciuchi, S. & Fratini, S. Electronic transport and quantum localization effects in organic semiconductors. *Phys. Rev. B* **86**, 245201 (2012).
13. Illig, S. et al. Reducing dynamic disorder in small-molecule organic semiconductors by suppressing large-amplitude thermal motions. *Nat. Commun.* **7**, 10736 (2016).
14. Eggeman, A. S., Illig, S., Troisi, A., Sirringhaus, H. & Midgley, P. A. Measurement of molecular motion in organic semiconductors by thermal diffuse electron scattering. *Nat. Mater.* **12**, 1045–1049 (2013).
15. Fukami, T. et al. Correlation between thermal fluctuation effects and phase coherence factor in carrier transport of single-crystal organic semiconductors. *Appl. Phys. Lett.* **106**, 143302 (2015).
16. Sakai, K. et al. The emergence of charge coherence in soft molecular organic semiconductors via the suppression of thermal fluctuations. *NPG Asia Mater.* **8**, e252 (2016).
17. Kubo, T. et al. Suppressing molecular vibrations in organic semiconductors by inducing strain. *Nat. Commun.* **7**, 11156 (2016).

18. Ren, Z. Q., McNeil, L. E., Liu, S. & Kloc, C. Molecular motion and mobility in an organic single crystal: Raman study and model. *Phys. Rev. B* **80**, 245211 (2009).
19. Aragó, J. & Troisi, A. Dynamics of the excitonic coupling in organic crystals. *Phys. Rev. Lett.* **114**, 26402 (2015).
20. Podzorov, V. Organic single crystals: addressing the fundamentals of organic electronics. *Mrs. Bull.* **38**, 15–24 (2013).
21. Goldmann, C. et al. Hole mobility in organic single crystals measured by a 'flip-crystal' field-effect technique. *J. Appl. Phys.* **96**, 2080–2086 (2004).
22. Reese, C., Chung, W.-J., Ling, M., Roberts, M. & Bao, Z. High-performance microscale single-crystal transistors by lithography on an elastomer dielectric. *Appl. Phys. Lett.* **89**, 202108 (2006).
23. Laudise, R., Kloc, C., Simpkins, P. & Siegrist, T. Physical vapor growth of organic semiconductors. *J. Cryst. Growth* **187**, 449–454 (1998).
24. Kloc, C., Simpkins, P. G., Siegrist, T. & Laudise, R. A. Physical vapor growth of centimeter-sized crystals of α-hexathiophene. *J. Cryst. Growth* **182**, 416–427 (1997).
25. Blülle, B., Troisi, A., Häusermann, R. & Batlogg, B. Charge transport perpendicular to the high mobility plane in organic crystals: bandlike temperature dependence maintained despite hundredfold anisotropy. *Phys. Rev. B* **93**, 35205 (2016).
26. Tavazzi, S. et al. Dielectric tensor of tetracene single crystals: the effect of anisotropy on polarized absorption and emission spectra. *J. Chem. Phys.* **128**, 154709 (2008).
27. Podzorov, V. et al. Intrinsic charge transport on the surface of organic semiconductors. *Phys. Rev. Lett.* **93**, 1–4 (2004).
28. De Wijs, G. A., Mattheus, C. C., De Groot, R. A. & Palstra, T. T. M. Anisotropy of the mobility of pentacene from frustration. *Synth. Met.* **139**, 109–114 (2003).
29. da Silva Filho, D. A., Kim, E.-G. & Brédas, J.-L. Transport properties in the rubrene crystal: electronic coupling and vibrational reorganization energy. *Adv. Mater.* **17**, 1072–1076 (2005).
30. Lee, J. Y., Roth, S. & Park, Y. W. Anisotropic field effect mobility in single crystal pentacene. *Appl. Phys. Lett.* **88**, 252106 (2006).
31. Reese, C. & Bao, Z. High-resolution measurement of the anisotropy of charge transport in single crystals. *Adv. Mater.* **19**, 4535–4538 (2007).
32. Sundar, V. C. et al. Elastomeric transistor stamps: reversible probing of charge transport in organic crystals. *Science* **303**, 1644–1646 (2004).
33. Wen, S. H. et al. First-principles investigation of anistropic hole mobilities in organic semiconductors. *J. Phys. Chem. B* **113**, 8813–8819 (2009).
34. Hannewald, K. et al. Theory of polaron bandwidth narrowing in organic molecular crystals. *Phys. Rev. B* **69**, 75211 (2004).
35. Ishii, H., Kobayashi, N. & Hirose, K. Strong anisotropy of momentum-relaxation time induced by intermolecular vibrations of single-crystal organic semiconductors. *Phys. Rev. B* **88**, 205208 (2013).
36. Dovesi, R. et al. CRYSTAL14: a program for the ab initio investigation of crystalline solids. *Int. J. Quantum Chem.* **114**, 1287–1317 (2014).
37. Campbell, R. B., Robertson, J. M. & Trotter, J. The crystal structure of hexacene, and a revision of the crystallographic data for tetracene. *Acta Crystallogr.* **15**, 289–290 (1962).
38. Allen, F. H. The Cambridge Structural Database: a quarter of a million crystal structures and rising. *Acta Crystallogr. Sect. B Struct. Sci.* **58**, 380–388 (2002).
39. Frisch, M. J. et al. *Gaussian 09* (Gaussian, Inc., Wallingford, 2016).
40. Merrick, J. P., Moran, D. & Radom, L. An evaluation of harmonic vibrational frequency scale factors. *J. Phys. Chem. A* **111**, 11683–11700 (2007).
41. Loudon, R. The Raman effect in crystals. *Adv. Phys.* **13**, 423–482 (1964).

Acknowledgements

The authors would like to thank Oleg Kirillov for assistance in fabricating photoresist masks and Lee Richter for discussions. Certain commercial equipment, instruments, or materials are identified in this paper in order to specify the experimental procedure adequately. Such identification is not intended to imply recommendation or endorsement by the National Institute of Standards and Technology, nor is it intended to imply that the materials or equipment identified are necessarily the best available for the purpose.

Author contributions

E.G.B. and D.J.G. conceived the project, E.G.B., A.J.B., A.A.H., and A.R.H.W. designed experiments, and L.A.F. and T.C.A. developed calculations. E.G.B. grew crystals, and designed, fabricated, and measured transistors. A.J.B. performed Raman measurements and determined crystal orientation. L.A.F. calculated the vibrational spectrum and HOMO interaction and created calculation visuals. A.A.H. performed TEM measurements. E.G.B. wrote the paper with input from all authors.

Additional information

Supplementary information accompanies this paper at https://doi.org/10.1038/s42005-019-0129-5.

Competing interests: The authors declare no competing interests.

Reprints and permission information is available online at http://npg.nature.com/reprintsandpermissions/

Publisher's note: Springer Nature remains neutral with regard to jurisdictional claims in published maps and institutional affiliations.